

Process redesign of complex forged parts with the strongly process-correlated index

Minye Cao¹, Chengliang Hu^{1,2,*} , Shengshi Li³, Zhen Zhao¹, and Chenyi Zhu⁴

¹ National Engineering Research Center of Die and Mold CAD, School of Material Science and Engineering, Shanghai Jiao Tong University, Shanghai 200030, PR China

² Inner Mongolia Research Institute, Shanghai Jiao Tong University, Inner Mongolia 010010, PR China

³ Hubei Tri-ring Forging Co., Ltd., Xiangyang 441700, PR China

⁴ Shanghai Aichi Forging Co., Ltd., Shanghai 201814, PR China

Received: 11 April 2025 / Accepted: 21 July 2025

Abstract. The forging processes of two typical complex parts were redesigned by using a strongly process-correlated index (SPCI) to achieve better quality and high productivity. This approach involves extracting the cross-sectional area of three-dimensional complex parts, characterizing the variation in this geometric feature using fractal dimension analysis, and computing the volume ratio between the minimum circumscribing cylindrical envelope of the forged part and the forged part itself. Six crankshaft variants were designed to further demonstrate the effectiveness of the SPCI, the larger the SPCI value the poorer the forgeability. To decrease the risk of crack defects on steering arm in T shape generated during the initial process, the forging process with smaller SPCI is redesigned. As expected, a more uniform velocity distribution can be found in critical areas from simulation results, and this will benefit to solve the problem of crack. For the four-cylinder crankshaft part, the SPCI is relatively large because of the quite different shape of the counterbalances. A redesign of combined two parts in one with a smaller SPCI was proposed and the forging process was double checked with simulation from the aspects of forging defects and the capability of forging press. The redesigned crankshaft forging was forged and two qualified crankshafts with required mechanical properties and dimensional accuracy were obtained in one shot.

Keywords: Strongly process-correlated index / forged parts / deformation degree / fractal dimension / process redesign

1 Introduction

The forging process, known for its advantages in enhancing material ductility, reducing waste, improving product performance, and increasing production efficiency, is now a widely utilized and efficient metal-forming technique within the manufacturing industry [1]. To promote the green development of forging technology, efficient process redesign or process optimization technology is needed to improve the forging process, thereby reducing forging defects and improving forging production efficiency.

Various factors such as tool temperature, slug geometry, press settings, process speed, lubrication, transportation time, and contact friction directly impact the forging process [2]. Consequently, considerable efforts have been devoted to optimizing process design to decrease forging

loads and minimize the risk of tool failure [3,4]. Since a trial-and-error approach is unsuitable for developing high-precision forging products due to significant development costs and time incurred, numerical models including the direct differentiation method [5], upper-bound methods [6,7], slab method [8], and slip-line field method [9] have been employed to analyze the forging process and design parameters. However, simplified mathematical models struggle to accurately depict the deformation process of complex parts. Therefore, finite element (FE) analysis was used to assist in the forging process design and parameter determination of complex parts in current days. The hot forging process of a spur bevel gear in magnesium alloy was investigated by FE simulations combined with experiment works [10]. With the aid of FE simulations, the forging process of a high-pressure common rail in 304 stainless steel was designed and introduced into mass production [11]. An innovative tool concept for forming small to medium batches of cost-competitive crankshafts was designed, and

* e-mail: clhu@sjtu.edu.cn

validated with test cases obtained from FE modeling and experimentation [12]. The effect of variations in different input parameters on the multi-stage hot forging process of a shackle was studied in details by modeling of the entire process with FE method [13,14].

What's more, when combined with different algorithms, the forging process was optimally designed based on the FE method. During an optimization procedure, which depends on the quality and cost requirements of the part, a suitable objective function is selected. The goal is to minimize the deformation energy [15], the number of forming stages [16], the difference between the desired shape and the final realized forged shape [17], the cost [18,19], the unfilled area of the die [20], the variation in hardness distribution [21], and the maximum strain rate to avoid folding defect [22]. These simulations provide detailed insights into material behavior under various conditions of stress, temperature, and deformation, thereby enabling the optimization of the forging process [23]. However, the optimal design of the process depends entirely on the accuracy of FE simulations, which are influenced by the availability of sufficient data for different boundary conditions.

Given the complexity of the forging process and the multitude of influencing factors, it is essential to establish a method for evaluating the complexity of a forging part prior to process design. Kinzle and Spies initially proposed a shape complexity factor based on the mass ratio of the forged part to that of a simple prismatic or cylindrical circumscribed shape [24], which allows for classifying most forged parts into three categories. Teterin et al. further advanced the concept by introducing a more practical and calculable complexity factor, which incorporates the perimeter and area of the forging's axial cross-section, the circumscribing cylinder's radius, and the distance from the symmetry axis to the center of gravity [25]. This factor was used to inform preform design, where contacting nodes on the preform are controlled based on results from backward deformation simulations [26].

For axisymmetric parts, four dimensionless parameters were introduced to evaluate the complexity of determining the optimal number of preform stages [27]. Tomov, focusing on rotationally symmetrical parts, evaluated complexity by comparing the work required during forging with that needed to forge an equivalent volume pancake, but with a different height determined by maintaining equal transformed volumes [28]. The need for a preform stage can also be estimated by comparing the relative deformation volumes of complex forgings to the logarithmic height strain observed during simple upsetting [29]. This approach was later expanded to non-rotational parts [30]. However, in such cases, the complexity factor could not be directly calculated.

In our previous work [31], the strongly process-correlated index can well evaluate the difficulty of the forging process and it was proved with several typical experimental and industrial case studies in axisymmetric forging parts. To extend the application, non-axisymmetric forgings with complex three-dimensional shapes are investigated in this work. The calculation method for the SPCI of three-dimensional complex parts was

illustrated using crankshafts as an example, and the SPCI was further discussed based on the forging simulation results of crankshaft variants. The SPCI was used to support the process redesign of two complex components. For the T-shaped steering arm, the improved redesign process could benefit to reduce the risk of cracking defects in the initial forging process. For the forging of the crankshaft, a two-part combined design with a smaller SPCI was proposed to facilitate easier forming. The forging process was then validated through both simulation and physical testing. As a result, the manufacturing process for these two complex forgings has become greener.

2 SPCI calculation for complex three-dimensional parts

The SPCI integrates two critical dimensions for evaluating forging complexity. First, adopting Kinzle and Spies' volumetric approach [24], SPCI calculates the ratio of circumscribing cylinder volume to forging volume. This ratio directly quantifies deformation severity: higher values indicate greater geometric complexity and more extensive material deformation during forming. Second, SPCI incorporates longitudinal cross-sectional area variation, which characterizes volume distribution and reflects required material transfer during forging – a parameter intrinsically linked to work done in deformation processes [28]. Increased fluctuation in this distribution corresponds to heightened shape complexity, quantified through fractal dimension analysis. The complete SPCI calculation follows the structured workflow in Figure 1.

The volume occupancy ratio, V_C/V_F was calculated for the complex parts. Here, V_F represents the volume of the forged part, and V_C denotes the volume of its minimum circumscribing cylindrical envelope. The distribution curve of the cross-sectional area along the longitudinal axis can depict variation of geometry for a complex forged part like crankshafts. By plotting the distribution curve of the cross-sectional area along the diameter of the forging, the geometric variations of the forging were effectively illustrated. To quantify the degree of volatility in these curves, the fractal dimension, a concept introduced by Mandelbrot et al., was employed [32]. The differential box-counting method, a straightforward mathematical technique, was used to calculate the fractal dimensions [33].

The fractal dimension of the distribution curve of the circumferential cross-sectional area was calculated by the differential box-counting method, noted as V_{geo} . The larger the value of V_{geo} , the greater the fluctuation in the distribution curve, which implies that the shape of the forging is more complex. The formula for calculating the fractal dimension of the tested curve is as follows [34]:

$$V_{geo} = \lim_{\varepsilon \rightarrow 0} \frac{\log(N(\varepsilon))}{\log(1/\varepsilon)}. \quad (1)$$

Where V_{geo} is the fractal dimension of the cross-sectional area distribution curve of the forged part, ε is the box size, and $N(\varepsilon)$ is the number of boxes at that size required to fully cover the analyzed curve.

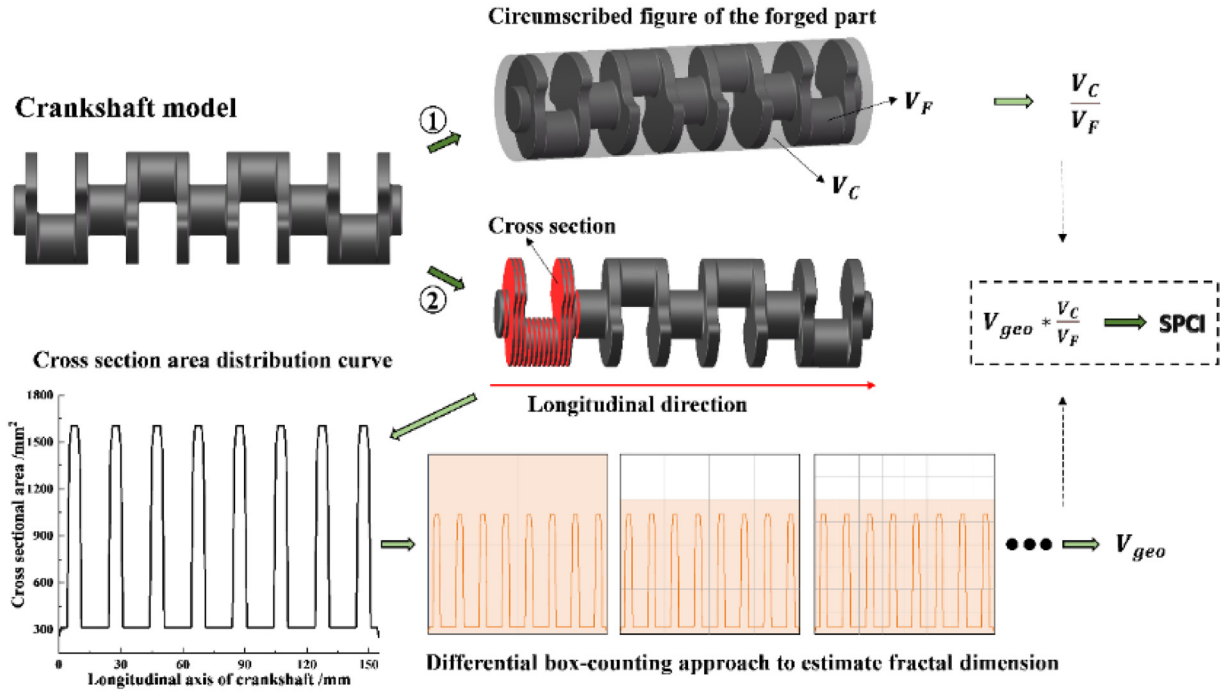


Fig. 1. Procedure for strongly process-correlated index calculation.

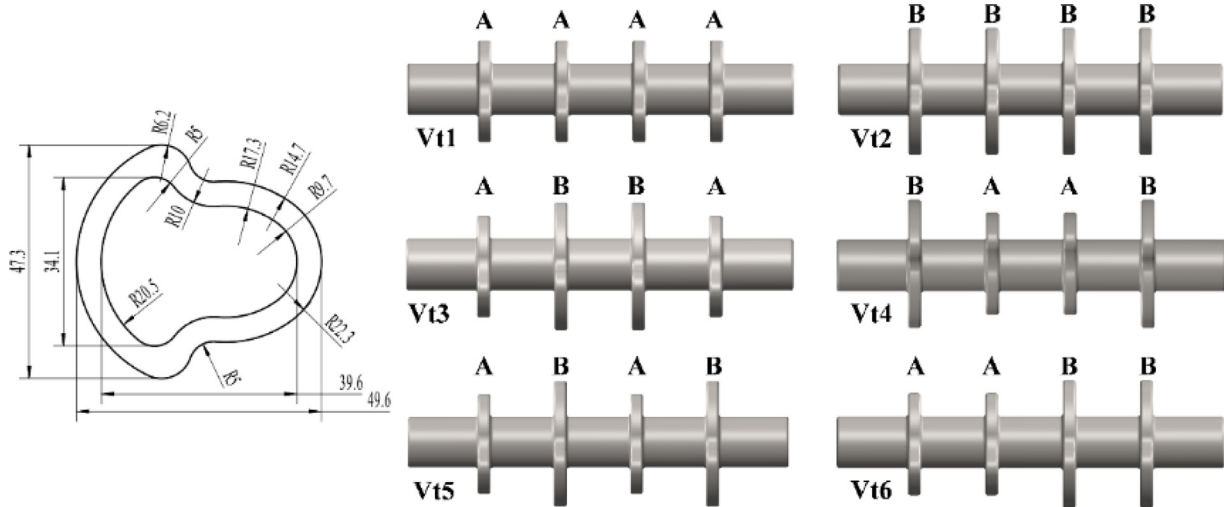


Fig. 2. Schematic diagram of counterbalances and crankshaft variants.

Under these conditions, the SPCI of three-dimensional complex parts was defined as follows:

$$SPCI = V_{geo} * \frac{V_C}{V_F} \tag{2}$$

The crankshaft, a representative example of complex parts, exhibits complexity in shape notably influenced by the size of its counterbalance. Six crankshaft variants with four counterbalances shown in the right of Figure 2 were designed to further demonstrate the effectiveness of the SPCI. For the specific dimension of the counterbalance, the small one Type A is defined with a height of 34.1 mm and a width of 39.6 mm, while the large one Type B is designed

with 47.3 mm in height and 49.6 mm in width, as detailed in Figure 1. Four counterbalances with same thickness of 5 mm were randomly positioned along a main bearing (20 mm in diameter and 150 mm in length).

As a result, the SPCI values of these six crankshaft variants are obtained as 3.57, 5.28, 5.09, 5.04, 5.23, and 5.02, respectively. Therefore, the order of complexity among the crankshaft variants can be determined as follows: $Vt1 < Vt6 < Vt4 < Vt3 < Vt5 < Vt2$.

To further evaluating the complexity, the forging processes of the six crankshaft variants are simulated, and the filling conditions, effective strain distribution, and forging load are analyzed. In FE model, the material TL1438 steel is selected from the material library, and the

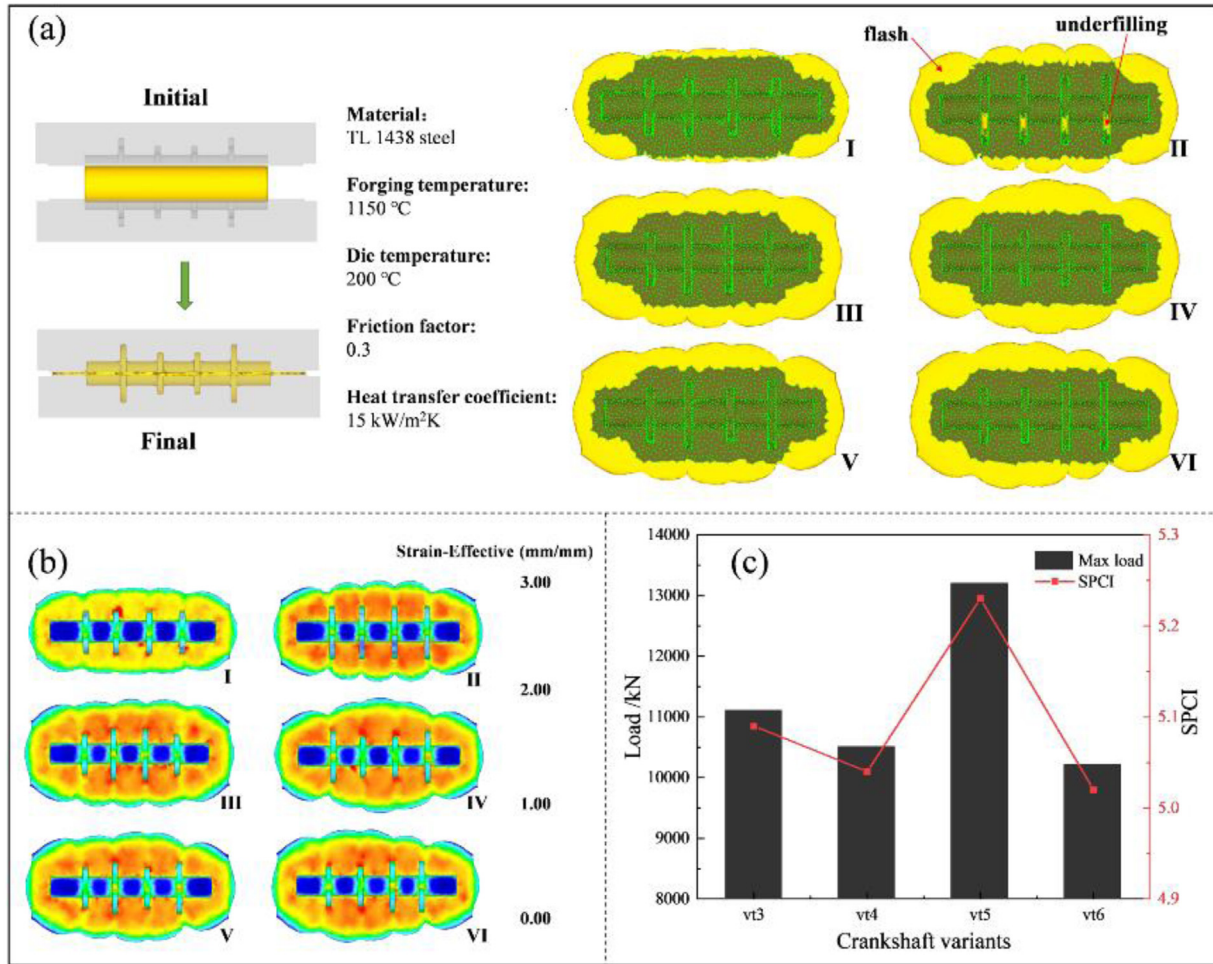


Fig. 3. Simulation results: (a) filling conditions, (b) effective strain field, (c) load maximum.

forging and die temperatures are set as 1150 °C and 200 °C, and the heat transfer coefficient and friction factor at the die-workpiece interface is defined as 15 kW/m²·K and 0.3, respectively [35,36]. To make it comparable, a uniform flash with a thickness of 2 mm of all the variants is set. The crankshaft variant was forged directly from a cylindrical billet, and the simulation results are presented in Figure 3.

The filling status of the forging die can be used as an indicator of the difficulty of forging. The complex parts are always difficult to be fully filled. As shown in Figure 3a, the underfilling can be found on the Vt2 crankshaft variant, and the others were all well-formed. The strain distribution can fully illustrate the deformation degree of forging parts. As depicted in Figure 3b, a quite non-uniform strain distribution can be observed because of the complex geometry of the crankshaft variants. The strain distributed on the Vt1 is significantly smaller than all the others, while the strain on Vt2 is slightly larger than the other four variants. This also shows that the SPCI can effectively capture the influence of deformation degree. To further analyze the differences between Vt3 to Vt6, the forging load-stroke curves are extracted in Figure 3c. The forging load reaches maximum in the end of the forging process. The

maximum of forging load of Vt3 to Vt6 are 11100, 10500, 13200, and 10200 kN, ranking as Vt6 < Vt4 < Vt3 < Vt5, consistently aligning with the order of the SPCI.

3 Process redesign of a T-shaped part

The steering knuckle arm is a key part for steering control in vehicles [37], and it is always designed in a T-shape. In mass production, on a typical T-shaped steering arm there is cracking defects. To solve this problem, the initial forging process need to be redesigned.

3.1 Defects of initial forging process

The specific shape and dimensions of the T-shaped steering arm are depicted in Figure 4a. The cross-sectional area along the longitudinal axis is present on Figure 4b, and the maximum and minimum sectional areas of the T-shaped arm are 7290 mm² at the straight hole end and 1577 mm² at the conical hole end, respectively. The ratio of cross-sectional area reaches 4.62, and this significant difference will inevitably cause substantial volume transfer and non-uniform material flow during the forging process. In the initial forging process, a rod workpiece of 42CrMo steel

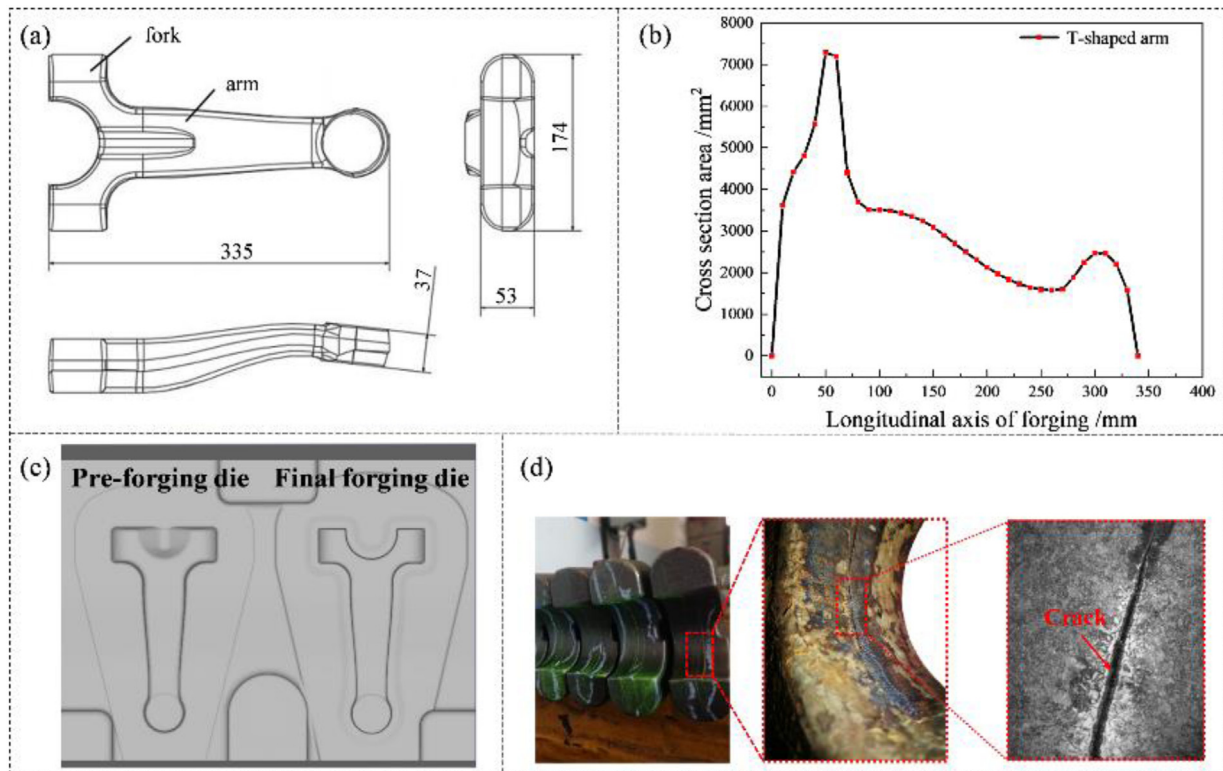


Fig. 4. (a) drawing of the T-shaped arm, (b) the cross-sectional area distribution curve, (c) forging die and (d) crack defects after forging.

with a diameter of 65.0 mm and a length of 412.0 mm was heated to 1180 °C and forged under a 2500 T forging press. Unfortunately, cracks appeared in the region identified in Figure 4d after final heat treatment. After forging, ultrasonic flaw detection revealed a defect rate exceeding 3.4%. When exacerbated during trimming, these minor defects could serve as precursors to cracks during subsequent heat treatments, potentially resulting in larger cracks and rendering the forging products unusable.

3.2 Process redesign of the T-shaped part

The drop of the T-shaped steering arm is 65.25 mm, which often leads to misalignment of the forging at the flash line. A horizontal force caused by die misalignment will be generated during the forging process, resulting in an increase of the eccentric die load and the non-uniform material flow. Therefore, the processes with two tryouts according to the concept of two pieces in one die are redesigned, the opposite arrangement of two forgings can reduce the misalignment force, and the corresponding forging dies involving with pre-forging and final forging are shown in Figures 5b and 5c. In the redesigned process I, the distance between the two pieces is 20 mm and the fork feature is prolonged to connect the two pieces in one forging, and there is a V-shaped splitting structure in the middle of the pre-forging die. In the redesigned process II, the distance between the two pieces is 40 mm and the area in between is set as a flash gutter.

According to the distribution curves of the cross-sectional area shown in Figures 4b, 5d, and 5e, the SPCI of the three different processes is determined to be 4.65, 4.35 and 5.05. Therefore, the redesigned process I can be selected as an improved forging scheme of the T-shaped steering arm.

3.3 Further analysis of improved redesign process

The forging processes of the redesigned and initial processes were simulated. As shown in Figure 6a, there is no underfilling and folding defects during the redesigned forging process, and the pre-forging and final forging loads were recorded as 2474 T and 3172 T, respectively. As reported in previous work [38], a non-uniform velocity distribution took place in the crack area, and the large velocity difference led to the generation of additional tensile stresses, and then resulted in crack formation. Similarly, five representative points at 10 mm intervals across the cross-section of the critical area were selected. The initial process exhibited an average velocity of 943.2 mm/s and a significant velocity difference of 1104.7 mm/s between points P1 and P5 (See Fig. 6c). This velocity disparity was the primary cause of crack defects in the fork area (See Fig. 4d). However, in the redesigned process an average velocity of 340.6 mm/s and a smaller velocity difference of 304.6 mm/s can be found (See Fig. 6b), and this more uniform material flow in the critical area could benefit to reduce the risk of cracks in the T-shaped forgings.

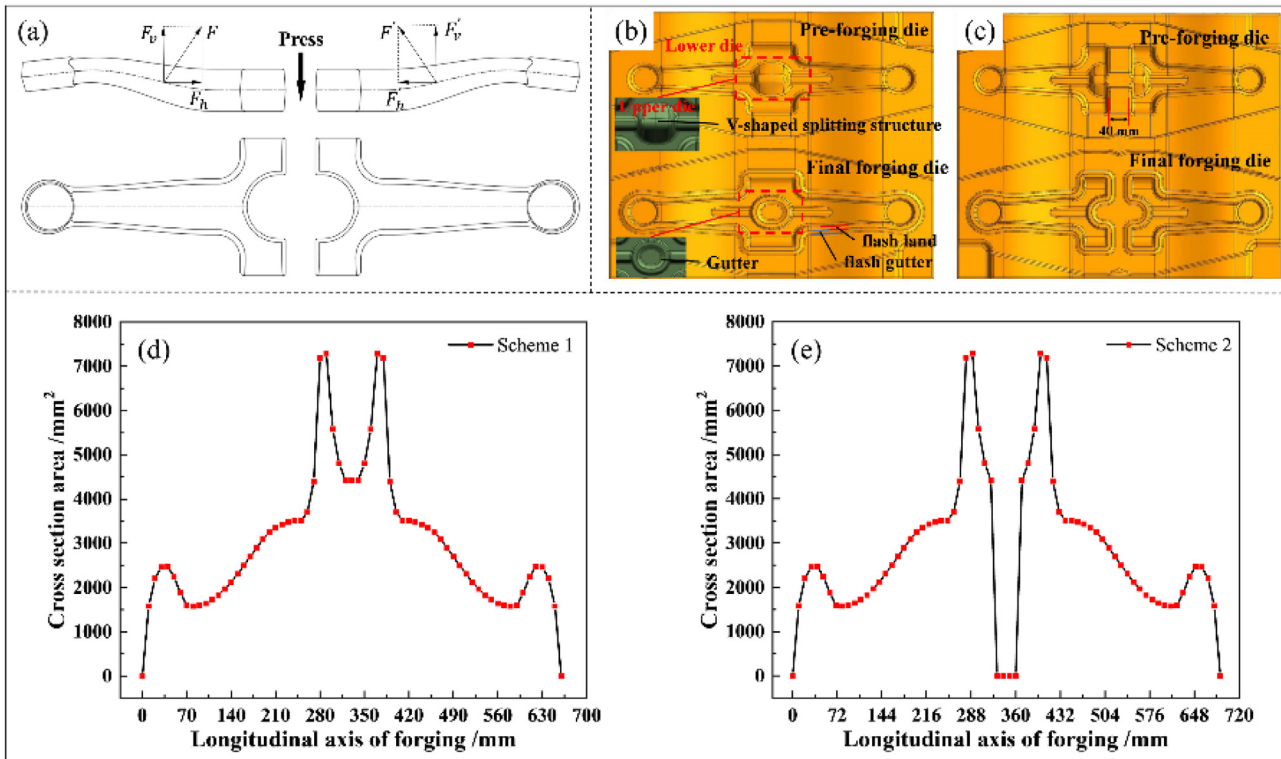


Fig. 5. Two pieces in one die of the T-shaped arm: (a) opposite arrangement, (b) forging die of the redesigned process I, (c) forging die of the redesigned process II, (d) the cross-sectional area distribution of the redesigned process I, (e) the cross-sectional area distribution of the redesigned process II.

In this case, the forging process for the T-shaped steering arm was redesigned using the SPCI. The redesigned process successfully addressed the crack defects present in the initial process, increasing the qualification rate of the forging parts. Additionally, the material utilization rate improved from 79.4% to 84.1%, achieving resource savings and enhancing energy efficiency.

4 Process design of complex crankshaft

Crankshafts are among the most critically loaded components in internal combustion engines, requiring superior mechanical properties [39]. Currently, the production of crankshafts predominantly employs open-die forging [40–42]. In this section, the SPCI for a four-cylinder crankshaft was found to be relatively high due to the distinct shape of its counterbalances. A two-part combined design with a smaller SPCI was then proposed, and the forging process was validated through simulation to check for potential forging defects and to assess the press capacity requirements.

4.1 Forging design considering the SPCI

As shown in Figure 7a, the key dimensions of the crankshaft in the three directions of length, width and height are 407.7 mm, 138.3 mm and 153.8 mm, respectively. Its cross-sectional area varies from 2291 mm² to

10978 mm², a difference of 4.8 times. The main chemical composition of its material is: C-0.40, Si-0.62, Mn-1.42, Cr-0.20, V-0.12, S-0.055, P-0.015, Al-0.017, N-0.015, the balance Fe (wt.%).

A large value of its SPCI is determined as 7.05 because of the quite different shape of the counterbalances. A redesign of combined two parts in one with a smaller SPCI of 6.62 is carried out. Additionally, damping grooves were added on the side of the die to prevent material overflow [38], as illustrated in Figure 7b. A flash thickness of 4 mm was set empirically. The forging process is double checked with simulation from the aspects of forging defects and the capability of forging press. To analyze this forging process, a simulation involving a round bar billet with a diameter of 95.5 mm and a length of 820.0 mm was conducted. The billet was heated to 1230 °C, and the forging dies were preheated to 250 °C. The heat transfer coefficient and friction factor at the die-workpiece interface were defined as 15 kW/m²K and 0.3, respectively.

4.2 Forging process analysis with simulation

As shown in Figure 8a, the temperature of the main body of the crankshaft part ranges from 1000 °C to 1150 °C after final forging, this relatively higher temperature distribution at this moment provides good temperature conditions for subsequent control cooling using the residual heat. As illustrated in Figure 8b, the large strain distributes at the flash area as expected because the main deformation already

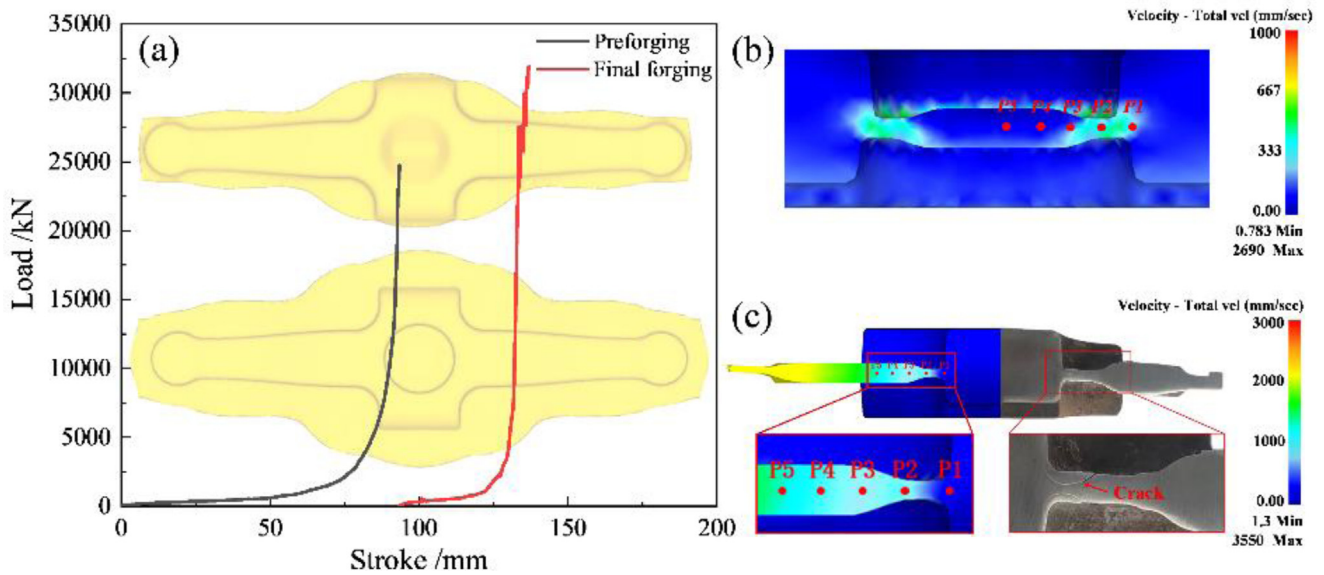


Fig. 6. (a) Stroke-load curve of improved process, (b) velocity distribution at the cross-section of improved process, and (c) velocity distribution at the cross-section of initial process.

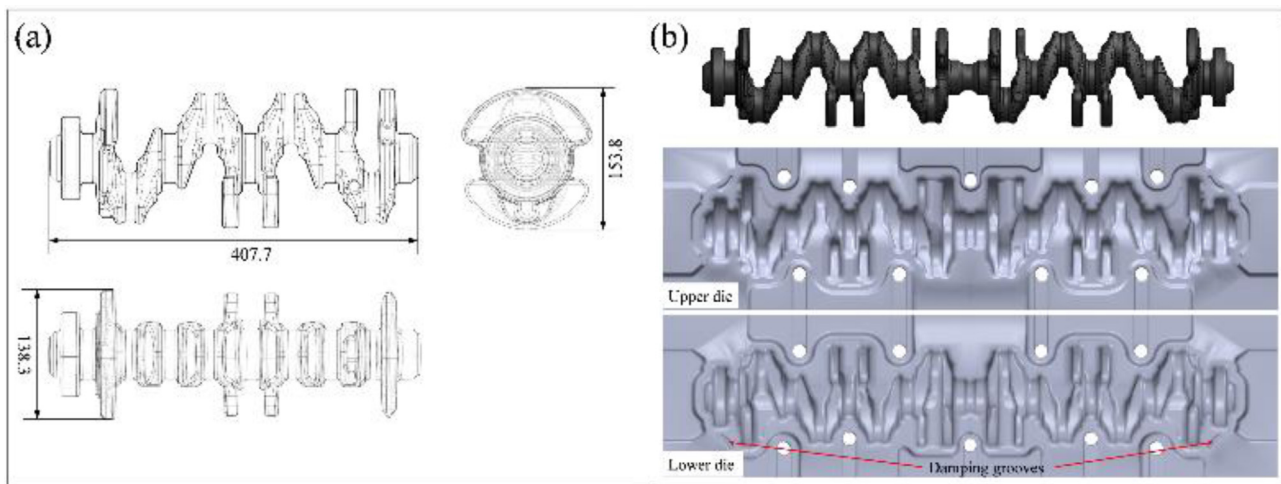


Fig. 7. (a) Structure diagram, and (b) two pieces in one die of the crankshaft.

occurs in the pre-forging stage, and the maximum strain reaches 3.6. What's more, the non-uniform metal flow results in folding at the flash edges indicated by the red circle on Figure 8b. However, these folding defects can be trimmed with the flash subsequently. With the help of damping grooves, the forging part of the crankshaft is fully filled as observed with the die contact status in Figure 8c. The predicted forging loads for the pre-forging and final forging were 4580 T and 5220 T, respectively, indicating that production can be carried out using the existing equipment.

The forging dies were designed, manufactured, and installed on a set of die bases, and the same-sized billet used in the finite element simulation was employed. The billet was heated up to 1230 °C by a medium frequency induction furnace, and the forging dies were pre-heated to 250 °C with an embedded die-heating system. The forging process was carried out on a 6300-ton crank press using a water-based

graphite lubricating system, and the forging loads of the pre-forging and final forging were recorded as 4800 T and 5500 T from the sensor integrated in the forging press, respectively. The forged part depicted in Figure 8d without forging defects like folding and underfilling is formed, demonstrating the effectiveness of the process design. After forging, the flash trimming process was performed a next press with a capability of 800 T.

4.3 Forging performance testing as required

After flash trimming, the crankshaft forgings were vertically suspended for air cooling due to the characteristics of non-quenched and tempered steel [43]. After control cooling, the crankshaft forgings were cut into two pieces, and then were sent to shot blasting to remove surface oxide scale. To control the quality of the forgings,

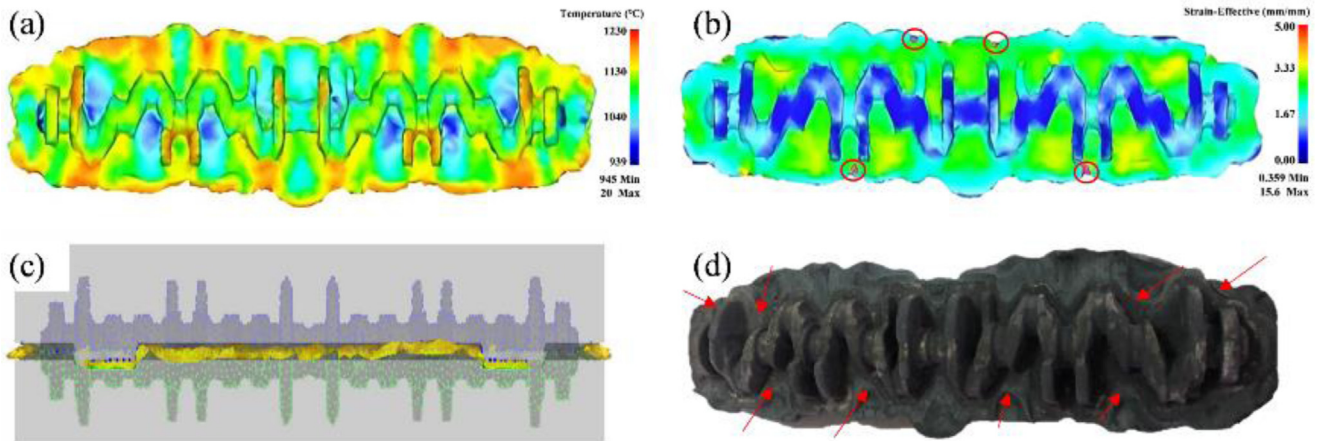


Fig. 8. Results of final forging: (a) temperature distribution, (b) strain distribution, (c) contact status, and (d) crankshaft forging.

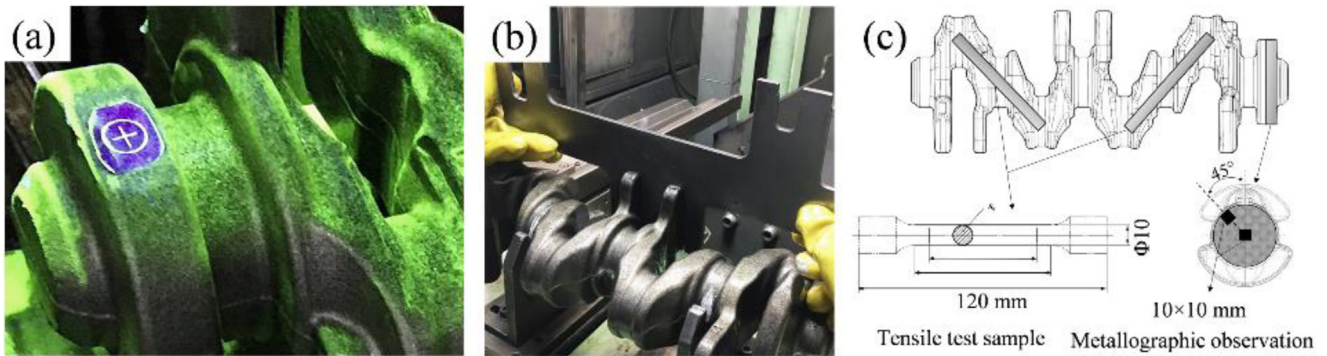


Fig. 9. Quality inspection of the forging: (a) magnetic particle testing, (b) dimensions measurement, and (c) performance testing.

magnetic particle inspection was performed. The testing results showed that there were no surface defects on the forged parts, as depicted in Figure 9a. The dimensions of the crankshaft part were assessed using a measuring tool depicted in Figure 9b for a quick check. No underfilling was observed, and crankshaft forgings with qualified dimensional accuracy were obtained.

Furthermore, mechanical properties and micro-grain characteristics were evaluated according to experimental specifications. Specimens for tensile testing and micro-structure analysis were extracted from multiple crankshaft forging zones, as documented in Figure 9c. Microstructural examination employed optical microscopy on mirror-polished specimens etched with 4% nitric acid, with grain size quantified through digital image processing. Tensile tests utilized an Instron 6800 series universal testing system at room temperature under constant 5 mm/min crosshead displacement control, with corresponding stress-strain curves presented in Figure 10.

The technical requirements for crankshaft include a yield strength higher than 580 MPa, a tensile strength higher than 850 MPa, an elongation greater than 12%, and a reduction of area greater than 25%. The average yield strength of the five samples was 615 MPa, the tensile strength was 915 MPa, and the elongation was 15%, with a reduction of area of 34%. The microstructure after control cooling was pearlite and ferrite, as depicted in Figure 11.

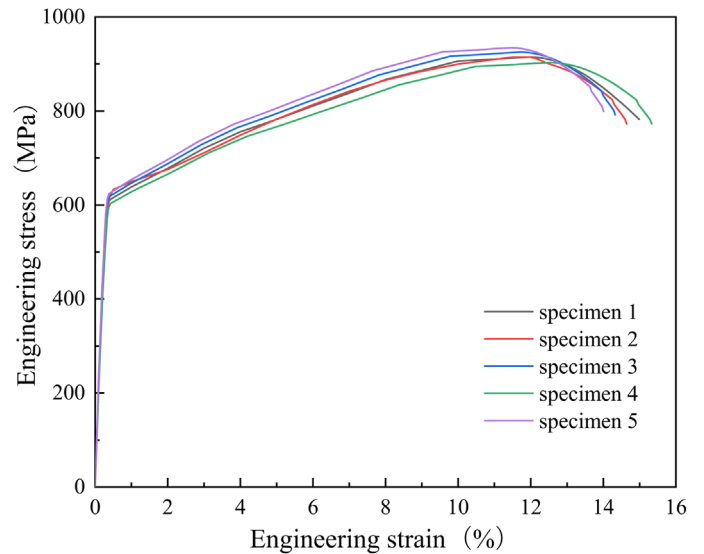


Fig. 10. Tensile stress-strain curves for the five specimens.

The microstructure indicated that the grain size grades of the core and surface area were all between grade 4.0 and grade 5.0, and no mixed crystal or coarse grains were observed.

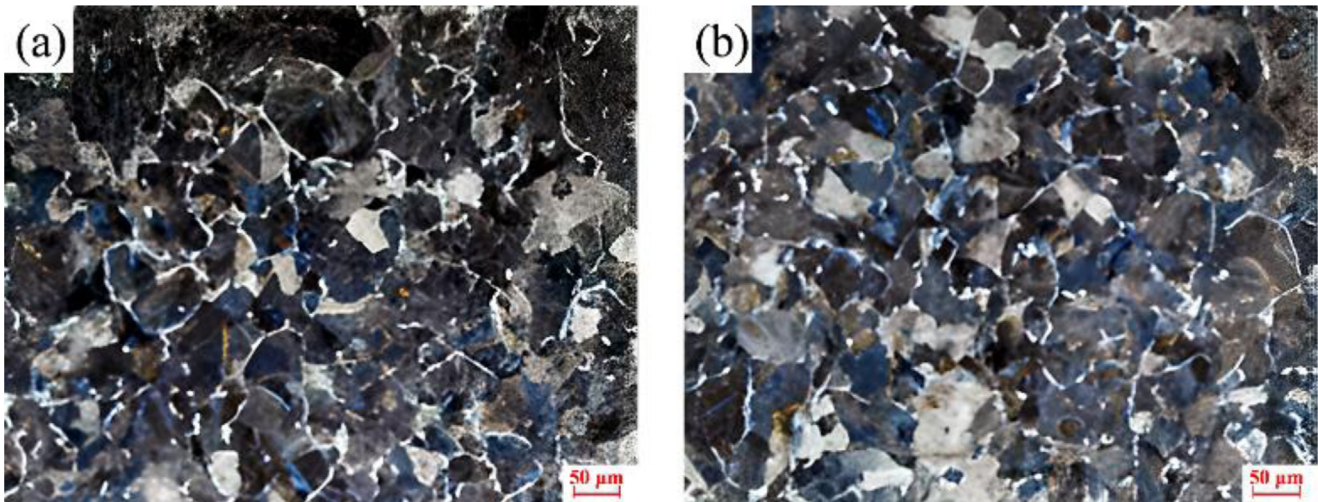


Fig. 11. Grain size of the crankshaft forgings at different positions: (a) surface, and (b) core.

In summary, to reduce the forging difficulty of a four-cylinder crankshaft, a two-part combined design was proposed by decreasing the SPCI from 7.05 to 6.62. The proposed process was carried out and qualified forgings with required dimension accuracy, mechanical properties in macro side and grain grade in microstructure were achieved. As for complex crankshafts, the forging design with smaller value of SPCI could benefit the successfully forging in practice. Additionally, the two-part combined design improved material utilization and production efficiency.

From the two industrial cases discussed above, the SPCI provides a quantitative quick tool to support the design selection for the forging process improvement or optimization. This rapid judge tool improves the efficiency of the forging process, especially for the complex three-dimensional components. In the next step, the application of SPCI to optimize of forging processes will be further investigated, potentially reducing or even replacing finite element simulations, thereby advancing intelligent manufacturing technologies for green forging of complex components.

5 Conclusions

- To evaluate the difficult of complex forging parts, the SPCI (strongly process-correlated index) was calculated following the definition in previous work. Different from axisymmetric forgings, the volume ratio is used to substitute the area ratio, and the cross-sectional area along the longitudinal axis is replaced by that along the diameter. Six crankshaft variants were designed to further demonstrate the effectiveness of the SPCI. A larger SPCI value corresponds to poorer forgeability.
- To address the crack defects observed in the T-shaped steering arm during the initial forging process, a redesigned forging process with a smaller SPCI was implemented. Comparative simulation results indicate that the redesign reduces the risk of cracks by promoting a more uniform velocity distribution in critical areas.
- For the four-cylinder crankshaft, a high SPCI value of 7.05 was determined due to the distinct shape of the counterbalances. A two-part combined design with a

lower SPCI of 6.62 was subsequently developed, and the forging process was verified through simulations to assess potential forging defects and the capability of the press. The redesigned crankshaft was ultimately forged on a 6300-ton crank press, yielding two crankshafts in a single step that met the required mechanical properties and dimensional accuracy.

- From the perspective of application, two aspects of this study warrant careful consideration in the future: additional industrial case studies are necessary to validate the effectiveness of the SPCI, given the complexities of real-world forging processes. An optimization approach or tool utilizing the SPCI, which may also incorporate additional optimization objectives, will be developed to facilitate the rapid optimization of forging processes.

Funding

This study was supported by the Project of High Precision Simulation Technology for Multi-directional Forging (GO0500093) and The Shanghai Explorer Program (24TS1413100).

Conflicts of interest

The authors declare that they have no known competing financial interests or personal relationships that could have appeared to influence the work reported in this paper.

Data availability statement

The data supporting this article is included within the article.

Author contribution statement

Minye Cao: Experiment, Analysis and Writing – original draft preparation; Chengliang Hu: Supervision, Analysis – review and editing; Shengshi li: Experiment – review and editing; Zhen Zhao: Analysis – review and editing; Chenyi Zhu: Experiment – review and editing;

References

1. M. Dalbosco, G. da Silva Lopes, P.D. Schmitt et al., Improving fatigue life of cold forging dies by finite element analysis: a case study, *J. Manuf. Process.* **64** (2021) 349–355
2. Z. Gronostajski, M. Hawryluk, The main aspects of precision forging, *Arch. Civ. Mech. Eng.* **8** (2008) 39–55
3. D.J. Politis, N.J. Politis, J. Lin et al., A review of force reduction methods in precision forging axisymmetric shapes, *Int. J. Adv. Manuf. Technol.* **97** (2018) 2809–2833
4. A.A. Emamverdian, S. Yu, C.P. Cao et al., Current failure mechanisms and treatment methods of hot forging tools (dies) – a review, *Eng. Fail. Anal.* **129** (2021) 105678
5. A. Srikanth, N. Zabarar, Shape optimization and preform design in metal forming processes, *Comput. Methods Appl. Mech. Eng.* **190** (2000) 1859–901
6. H. Cho, J. Choi, G. Min et al., An upper-bound analysis of the closed-die forging of spur gears, *J. Mater. Process. Technol.* **67** (1997) 83–88
7. W. Yeh, M.C. Wu, A variational upper-bound method for analysis of upset forging of rings, *J. Mater. Process. Technol.* **170** (2005) 392–402
8. D.W. Zhang, H. Yang, Z.C. Sun, Analysis of local loading forming for titanium-alloy T-shaped components using slab method, *J. Mater. Process. Technol.* **210** (2010) 258–266
9. G. Samolyk, Z. Pater, Application of the slip-line field method to the analysis of die cavity filling, *J. Mater. Process. Technol.* **153–154** (2004) 729–735
10. J. Liu, Z.S. Cui, Hot forging process design and parameters determination of magnesium alloy AZ31B spur bevel gear, *J. Mater. Process. Technol.* **209** (2009) 5871–5880
11. M.Y. Cao, C.L. Hu, X.W. Zhuang et al., Study on the manufacturing process for enhancing the high-pressure capability of stainless-steel common rails, *Int. J. Adv. Manuf. Technol.* **127** (2023) 2447–2463
12. L.M. Alves, P.A.F. Martins, Flexible forming tool concept for producing crankshafts, *J. Mater. Process. Technol.* **211** (2011) 467–474
13. J. Cochet, S. Thuillier, P.Y. Manach et al., Thermo-mechanical forming of a large sling shackle, *Int. J. Adv. Manuf. Technol.* **86** (2016) 1573–1591
14. J. Cochet, S. Thuillier, N. Decultot et al., Investigation of the key process parameters in the hot forming of a shackle, *Int. J. Adv. Manuf. Technol.* **105** (2019) 3209–3219
15. M.H.A. Bonte, L. Fourment, T. Do et al., Optimization of forging processes using finite element simulations: a comparison of sequential approximate optimization and other algorithms, *Struct. Multidisc. Optimiz.* **42** (2010) 797–810
16. R. Hino, A. Sasaki, F. Yoshida et al., A new algorithm for reduction of number of press-forming stages in forging processes using numerical optimization and FE simulation, *Int. J. Mech. Sci.* **50** (2008) 974–983
17. Z. Kang, Y. Luo, Sensitivity analysis of viscoplastic deformation process with application to metal preform design optimization, *Eng. Optimiz.* **44** (2012) 1511–1523
18. V. Janakiraman, R. Saravanan, Concurrent optimization of machining process parameters and tolerance allocation, *Int. J. Adv. Manuf. Technol.* **51** (2010) 357–369
19. M. Ozturk, S. Kocaoglan, F.O. Sonmez, Concurrent design and process optimization of forging, *Comput. Struct.* **167** (2016) 24–36
20. D.J. Kim, B.M. Kim, J.C. Choi, Determination of the initial billet geometry for a forged product using neural networks, *J. Mater. Process. Technol.* **72** (1997) 86–93
21. H. Tumer, F.O. Sonmez, Optimum shape design of die and preform for improved hardness distribution in cold forged parts, *J. Mater. Process. Technol.* **209** (2009) 1538–1549
22. D. Vieilledent, L. Fourment, Shape optimization of axisymmetric preform tools in forging using a direct differentiation method, *Int. J. Numer. Meth. Eng.* **52** (2001) 1301–1321
23. S. Sharma, M. Sharma, V. Gupta et al., A systematic review of factors affecting the process parameters and various measurement techniques in forging processes, *Steel. Res. Int.* **94** (2023) n/a
24. O. Kinzle, K.V. Spies, Die Gestaltung der Zwischenformen für Gesenkschmiedestücke, *Werkstattstechnik und Maschinenbau*, Vol. **47**, 1957, pp. 175–181 (in German)
25. G.P. Teterin, I.J. Tarnovsky, A.A. Chechik, Criterion of complexity of the configuration of forgings, *Kuznechno Shtanmpovochnoe Proizvodstvo*, **7** (1966) 6–8 (in Russian)
26. G.Q. Zhao, E. Wright, R.V. Grandhi, Forging preform design with shape complexity control in simulating backward deformation, *Int. J. Mach. Tool. Manuf.* **35** (1995) 1225–1239
27. R. Hosseini-Ara, P. Yavari, A new criterion for preform design of H-shaped hot die forging based on shape complexity factor, *Int. J. Mater. Form.* **11** (2018) 233–238
28. B. Tomov, A new shape complexity factor, *J. Mater. Process. Technol.* **92** (1999) 439–443
29. B. Tomov, R. Radev, An example of determination of preforming stages in hot die forging, *J. Mater. Process. Technol.* **157** (2004) 617–619
30. B. Tomov, R. Radev, Shape complexity factor for closed die forging, *Int. J. Mater. Form.* **3** (2010) 319–322
31. M.Y. Cao, C.L. Hu, B.X. Cai et al., Complexity index of axisymmetric parts in the forging process based on variation in geometric changes, *Int. J. Adv. Manuf. Technol.* **135** (2024) 203–217
32. B.B. Mandelbrot, D.E. Passoja, A.J. Paulley, Fractal character of fracture surfaces of metals, *Nature* **308** (1984) 721–724
33. N. Sarkar, B.B. Chaudhuri, An efficient differential box-counting approach to compute fractal dimension of image, *IEEE Trans. Syst. Man. Cybern.* **24** (1994) 115–120
34. U. Freiberg, S. Kohl, Box dimension of fractal attractors and their numerical computation, *Commun. Nonlinear. Sci.* **95** (2021) 105615
35. W.H. Zhuang, X.H. Han, L. Hua et al., FE prediction method for tooth variation in hot forging of spur bevel gears, *J. Manuf. Process.* **38** (2019) 244–255
36. M.C. Chen, C.D. Zhu, Z.Q. Yu et al., A novel process for manufacturing large-diameter thin-walled metal ring: double-roll pendulum hot rotary forging technology, *J. Manuf. Process.* **76** (2022) 379–396
37. K. Reza Kashyzadeh, Effects of axial and multiaxial variable amplitude loading conditions on the fatigue life assessment of automotive steering knuckle, *J. Fail. Anal. Prev.* **20** (2020) 455–463
38. C.L. Hu, F. Zeng, Z. Zhao et al., Process optimization for design of duplex universal joint fork using unequal thickness flash, *Int. J. Precis. Eng. Manuf.* **16** (2015) 2517–2527

39. F.S. Silva, Analysis of a vehicle crankshaft failure, *Eng. Fail. Anal.* **10** (2003) 605–616
40. M. Churl Song, C.J. VanTyne, J. Rae Cho et al., Optimization of preform design in Tadeusz Rut forging of heavy crankshafts, *ASME J. Manuf. Sci. Eng.* **139** (2017) 091014
41. M. Meyer, M. Stonis, B.A. Behrens, Cross wedge rolling of preforms for crankshafts, *Key. Eng. Mater.* **504** (2012) 205–210
42. X. Wang, Z. Qi, K. Chen et al., Study on the forming accuracy of the three-cylinder crankshaft using a specific die with a preformed dressing, *Int. J. Adv. Manuf. Technol.* **104** (2019) 551–564
43. B. Jiang, W. Fang, R.M. Chen et al., Mechanical properties and microstructural characterization of medium carbon non-quenched and tempered steel: microalloying behavior, *Mat. Sci. Eng. A-Struct.* **748** (2019) 180–188

Cite this article as: Minye Cao, Chengliang Hu, Shengshi Li, Zhen Zhao, Chenyi Zhu, Process redesign of complex forged parts with the strongly process-correlated index, *Manufacturing Rev.* **12**, 21 (2025), <https://doi.org/10.1051/mfreview/2025016>